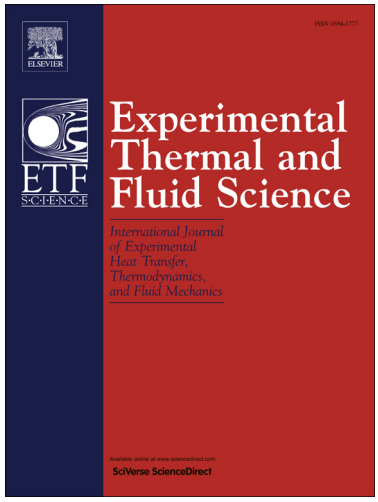

On the Mechanisms of Cavitation Erosion – Coupling High Speed Videos to Damage Patterns

Matevž Dular, Martin Petkovšek

PII: S0894-1777(15)00150-8
DOI: http://dx.doi.org/10.1016/j.expthermflusci.2015.06.001
Reference: ETF 8489

To appear in: *Experimental Thermal and Fluid Science*

Received Date: 20 March 2015
Revised Date: 1 June 2015
Accepted Date: 1 June 2015

Please cite this article as: M. Dular, M. Petkovšek, On the Mechanisms of Cavitation Erosion – Coupling High Speed Videos to Damage Patterns, *Experimental Thermal and Fluid Science* (2015), doi: http://dx.doi.org/10.1016/j.expthermflusci.2015.06.001

On the Mechanisms of Cavitation Erosion – Coupling High Speed Videos to Damage Patterns

Matevž Dular (corresponding author)
Laboratory for Water and Turbine Machines
Faculty of Mechanical Engineering
University of Ljubljana
Askerceva 6
1000 Ljubljana
SI-Slovenia

E-mail: matevz.dular@fs.uni-lj.si
Phone: +386 1 4771 453
Fax: +386 1 2518 567

Martin Petkovšek
Laboratory for Water and Turbine Machines
Faculty of Mechanical Engineering
University of Ljubljana
Askerceva 6
1000 Ljubljana
SI-Slovenia

Abstract

Recently van Rijsbergen et al. [1], by simultaneous observation of cavitation and acoustic emission measurements, and Petkovsek & Dular [2], by simultaneous observation of both cavitation structures and cavitation damage, have pointed to the fact that the small scale structures and the topology of the cavitation clouds play a significant role in cavitation erosive potential. Despite the two, before mentioned, studies opened some new insights to the physics of cavitation damage, many new questions appeared. In the present study we attached a thin aluminum foil to the surface of a transparent Venturi section using two sided transparent adhesive tape. The surface was very soft – prone to be severely damaged by cavitation in a very short period of time. Using high speed cameras, which captured the images at 30000 frames per second, we simultaneously recorded cavitation structures (from several perspectives) and the surface of the foil. Analysis of the images revealed that five distinctive damage mechanisms exist – spherical cavitation cloud collapse, horseshoe cavitation cloud

collapse, the “twister” cavitation cloud collapse and in addition it was found that pits also appear at the moment of cavitation cloud separation and near the stagnation point at the closure of the attached cavity.

Key words: Cavitation; Erosion; Mechanisms; Cavitation Cloud; Separation; Closure

1 Introduction

Briefly, cavitation is the occurrence of vapour cavities inside a liquid. It is well known that in static conditions a liquid changes to vapour if its pressure is lowered below the so-called vapor pressure. In liquid flows, this phase change is generally due to local high velocities which induce low pressures. The liquid medium is then "broken" at one or several points and "voids" appear, whose shape depends strongly on the structure of the flow [3]. Cavitation and consequently cavitation erosion is one of the most ubiquitous problems at operation of turbines, pumps, ship propellers and valves.

The general behavior of the developed cavitating flow follows a distinctive pattern where cavitation structures of different shapes and sizes are shed from the attached cavity (Fig. 1).

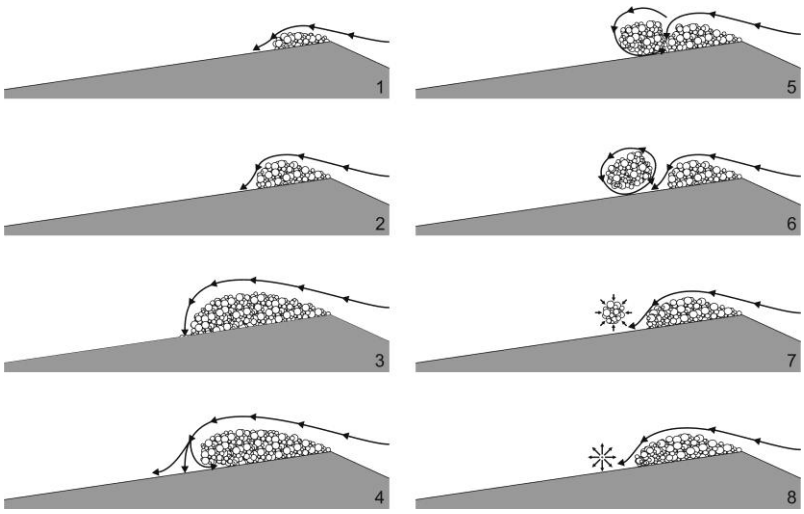

Figure 1: The shedding of cavitation clouds (the inner structure and the size of the bubbles may not correspond to reality).

The pressure difference between the outer flow and the inside of the attached cavity, forces the streamlines to curve towards the cavity and the surface beneath it. This causes attached cavity to close and the formation of a stagnation point at which the flow is split into outer flow which reattaches to the wall and the re-entrant jet which travels upstream, carrying a small quantity of the liquid to the inside the cavity. As the re-entrant jet travels upstream it looses momentum due to shear forces, turns upwards and "cuts" the attached cavity, causing cavitation cloud separation (shedding). The cloud is then entrained downstream by the main flow and can violently collapse in a region of pressure recovery. During the separation, circulation around the structure appears, causing it to reshape, break up etc. Meanwhile the attached cavity begins to grow and the process is periodically repeated [4].

In the past, cavitation shedding process and its relation to the erosive potential of cavitation was frequently discussed. Reisman et al. [5] suggested that the formation, focusing and propagation of shock waves, emitted at macroscopic structures collapse play a critical role in generating the pressure pulses which lead to cavitation noise and damage. Bark et al. [6] pointed to the spherical cavitation cloud collapse, where the converging flow enables efficient focusing of the energy which increases as the collapse proceeds and is finally converted into acoustic energy in the cavity collapse, associated with the radiation of shock waves. Foeth et al. [7] have shown that the cloud cavitation that is associated with the break up of sheet cavitation is essentially an organized mixture of cavitating vortices. Boorsma & Whitworth [8] and van Rijsbergen et al. [1] related the structures to the acoustic emission signals and suggested that the orientation of the shock wave should be considered. Large scale primary spanwise vortices were studied by Pereira et al. [9] and Kawanami et al. [10], who observed their development by stereography and holography, respectively. They have shown that the focusing of the collapse could play a role in the aggressiveness of erosion.

All the mentioned studies agree that cavitation structures carry a significant amount of potential energy [11] and can, at their collapse, emit pressure waves of magnitude of several MPa [12]. Yet it seems that the macroscopic

cavitation cloud collapse itself cannot be a direct cause of erosion as its energy is not enough concentrated. Currently the most widely accepted explanation of the phenomenon is that the potential energy contained in a macro-cavity transformed into the radiation of acoustic pressure waves, and further on into the erosive power contained in the micro-scale cavitation structures or single bubbles that collapse in the vicinity of the material boundaries [13, 14].

One can acknowledge a vast variety of studies that have addresses the physical background of cavitation erosion phenomenon. However, obviously, many questions remain open. Recent studies by van Rijsbergen et al. [1] and Petkovsek & Dular [2] hypothesized that it is either i) that the number and the distribution of the single bubbles in the vicinity of the wall have a mayor role in the process of cavitation erosion or ii) that the shock waves that originate from the cloud collapse are not perfectly spherical and have a clear orientation – the highest impact occurs when the wave front is directed toward the wall. The original motivation behind the present study was to gain a more in-depth knowledge of the process and the either confirm or deny the mentioned hypotheses. As the work progressed we realized that probably neither hypothesis is valid since a much more diverse dynamics as anticipated was observed – the focus of the study then focused to isolation of different phenomena that caused damage to the material.

In the present study the types of macro-cavities or the origins of damage occurrence are discussed. High speed cameras were used to simultaneously record the sequences of the cavitation dynamics and the damage sustained on the surface of the solid body. It is shown that the shedding process can evolve in different ways, leading to various hydrodynamic mechanisms that eventually converge to extreme conditions that can trigger events on a micro-scale that cause erosion. The results are valuable for future development of cavitation erosion prediction methods [15].

2 Experimental set-up

Cavitation tests were performed in a small cavitation tunnel at the Laboratory for Water and Turbine Machines,

University of Ljubljana.

The experimental procedure was essentially the same as in our previous study [2] where it is described in more detail. In the following only a brief description with key features is given.

2.1 Experimental set-up and the Venturi geometry

Erosion was studied in a Venturi geometry (Fig. 2), which was 10 mm wide with a converging angle of 18º and diverging angle of 8º (Fig. 2). The throat dimensions were $10\times10mm^2$. The test section was made out of transparent plexi glass so that observation from all directions was made possible.

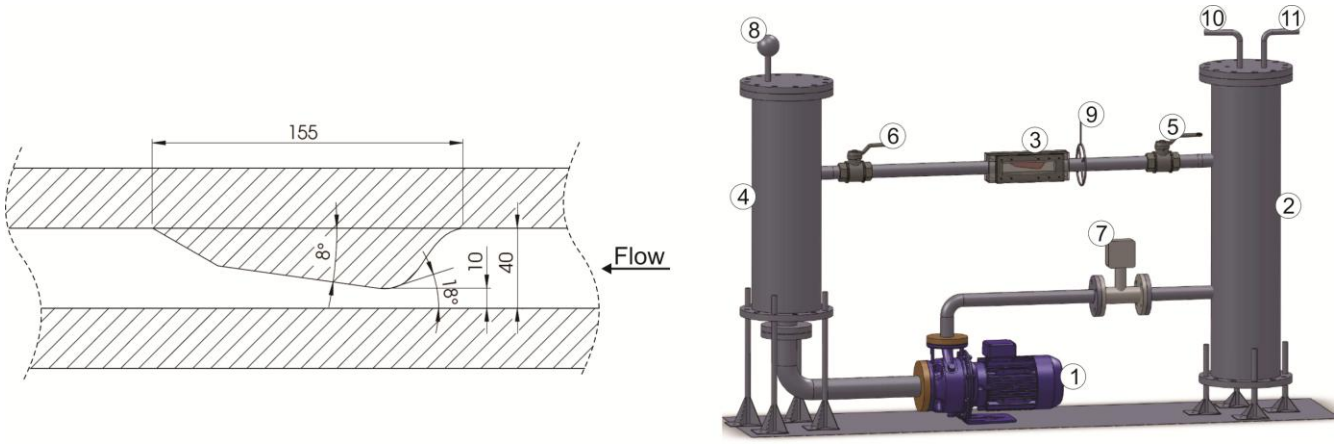

Figure 2: The Venturi geometri (left) and the experimental setup (right): (1) Pump, (2) upstream tank, (3) test section, (4) downstream tank, (5 and 6) valves, (7) electromagnetic flow meter, (8) thermocouple, (9) pressure sensor, (10) compressor and (11) vacuum pump.

The section was mounted into a cavitation tunnel (Fig. 2 right) with a closed loop circle what enables to vary both the flow rate and the system pressure. This way a wide range of operating points can be achieved. These are usually defined by the cavitation number:

$$\sigma = \frac{p_\infty - p_v}{\frac{1}{2}\rho v^2} \quad . \qquad (1)$$

which is given by the difference between the reference and vapour pressure divided by the dynamic pressure (given by the liquid density and the reference flow velocity).

The idea was to obtain sufficient damage in a very short period of time (in about 1 second). To set the operating conditions, first the test rig pressure was set to a desired value (490000 Pa, absolute pressure), then the valve upstream of the test section was closed and the pump was switched on to a determined rotating frequency. As the upstream valve was rapidly opened the velocity increased from 0 to 27.4 m/s in about 0.05 s achieving cavitation number $\sigma = 1.3$. The rapid setting of the desired operating point was necessary to decrease the possibility of severely damaging of the foil before the start of the image acquisition. It needs to be noted that all results presented later on were all obtained at the same operating conditions, and are therefore not dependent on the flow parameters. To increase the aggressiveness of cavitation the water was degassed by running the test rig at a low pressure for 30 minutes. In order to assure repeatable measurements the quantity of the dissolved gases was measured by the Van-Slyke method [16] – the increase of the dissolved gases is proportional to the increase of the cavitation nuclei content [17, 18]. The gas content of 15 mg of gases per liter of water was constantly measured.

2.2 Aluminum foil as an erosion sensor

The idea of the experiment was to simultaneously record images of cavitation structures and cavitation erosion. The upper side of the foil is covered by vapour structures that obstruct the view, hence one needs to look at the foil from the bottom side to see the damage. Consequently the whole test section had to be made of transparent material and, equally important, the foil had to be thin enough so that the cavitation damage, which occurs on the side exposed to cavitation was also visible on the other side. We have chosen 10 μm thick aluminum foil and

attached it to a Venturi section by a transparent two sided adhesive tape with thickness of 50 μm (Fig. 2).

2.3 Image acquisition

Two cameras were used in the experiment (Fig. 3). For the present experiment they were synchronized and recorded at 30000fps at a reduced resolution.

For observation of the aluminum foil we used a high speed camera Motion Blitz EoSens mini 1. It was looking at the foil from the back side (through the Venturi structure) and positioned in an axis perpendicular to the foil (ERO). The resolution of capturing was 288×90 pixels, giving the pixel size of 0.111 mm (the region of interest extended over 32×10 mm).

Two positions were used for the second camera – the Fastec Imaging HiSpec4 2G mono. It was either positioned above the Venturi, looking at the cavitation from the top (CAV-1) or from a side (somewhat perspective) view (CAV-2). Positioning the camera in a slightly perspective view (at a bit downstream side of the channel) revealed some 3 dimensional topological features of the cavitation structures. Images of cavitation were recorded at a resolution of 608×64 pixels for the top view, and at 448×86 pixels for the perspective view.

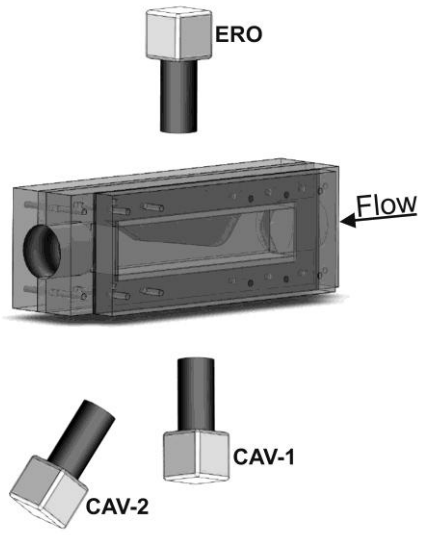

Figure 3: The directions of observation.

2.4 Damage evaluation

Since we are observing the foil with a camera only the surface of the damaged area can be accurately measured. Images of the aluminum foil were treated as matrixes with i×j (288×90) elements ($A(i,j) \in \{0,1,\ldots 255\}$) with values which can range from 0 (black) to 255 (white). Erosion was evaluated in image pairs: image matrix at time $t+\Delta t$ was subtracted from image matrix at time t ($B(i,j,t)= A(i,j,t) - A(i,j,t+\Delta t)$). This way a new matrix B was obtained. When the matrix element B(i,j) did not change between times t and $t+\Delta t$ its value was 0 ($B(i,j,t)=0$). When change occurred the value was $B(i,j,t)\neq 0$. Since small changes could be present due to insignificant changes in illumination, vibration etc., damage was only considered when a certain change threshold was exceeded ($B(i,j,t)>12$; this corresponds to more than 5% of decrease in brightness – pits always appeared as dark regions). The number of the pits, their size and overall damaged area could then be easily determined (Fig. 4).

Figure 4: Manipulation of the images of the damaged surface. From each image pair we obtained the number and the area of newly appeared pits (at $t+\Delta t$).

The method gives a distribution of the number and the area of the pits and consequently, the distribution of the magnitude of cavitation erosion on the surface. We could also determine the distribution of the size of the pits. Since we were comparing pairs of two successive images we were also able to consider the possibility of pit overlapping.

3 Results

A typical damage occurs in form of a pit, roughly 0.1mm in diameter. Following an event (for example cavitation cloud collapse) usually only a single pit occurred, though some mechanisms (especially the horseshoe

vortex collapse) frequently caused appearance of multiple pits. 4 typical examples of the pit appearance are shown in Fig. 5.

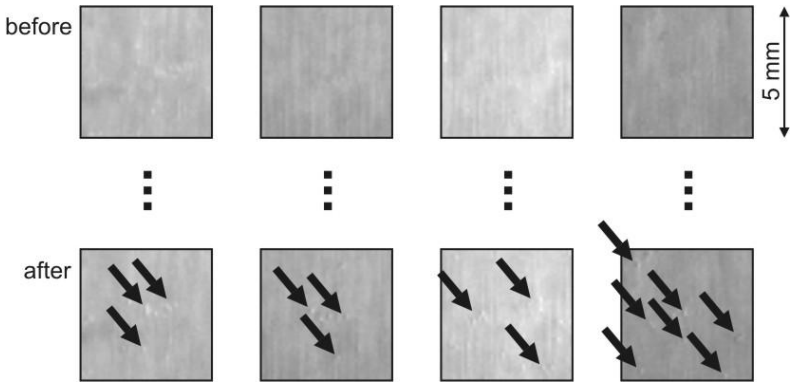

Figure 5: The pits appear as slightly darker areas, roughly 0.1mm in diameter.

It is obvious from observing the images in Fig. 5 that the pits can only be distinguished by comparing pairs of images using the technique described before (Section 2.4).

In the following we present the results of extensive image analysis. In the process, first the instant of the damage occurrence was determined. Then the evolution of cavitation structures during this period was analyzed and correlations between the two were investigated.

Not less than 5 different hydrodynamic phenomena that lead to the formation of the pit were determined, although it is possible that the physical background of some is more or less the same.

In Figs. 6 to 10 the dotted lines denote the boundaries of the channel, the damage (in images at t=0 ms) is enlarged for better representation and appears smaller in reality (its position and shape is not altered). The flow is always from the right to the left.

3.1 Spherical cavitation cloud collapse

Most often erosion is associated with the collapse of primarily cloud cavitation, referring to the fact that collective collapses of interacting bubbles in the cloud are shown to be very effective in focusing collapse energy

into a small spot, and typically generate significantly larger collapse pulse amplitudes than singly connected cavities. According to the energy cascade approach [6] the pressure waves emitted at the cloud collapse spread and cause implosion of micro-scale single bubbles in the vicinity of solid structures – causing pitting and eventually erosion.

Figure 6 shows two sequences of almost spherical cavitation cloud implosion from side (left) and top view (right).

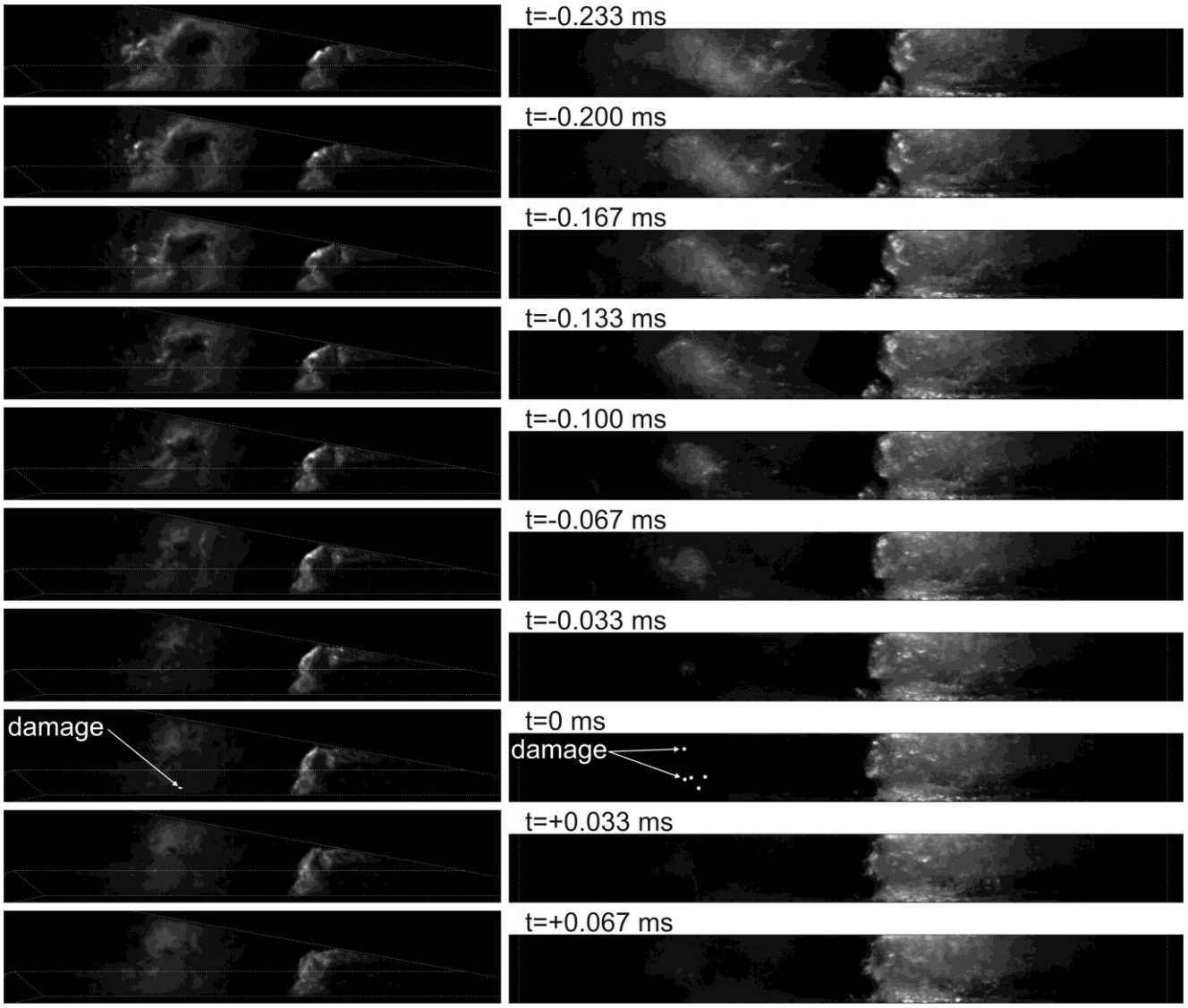

Figure 6: Collapse of a spherical cavitation cloud from side (left) and top view (right).

The sequences on the left and the right were not recorded simultaneously but they do represent the same phenomenon that leads to the damage.

Before the beginning of the sequence the re-entrant jet caused the separation of the cavity from the attached vapour structure. At that point no (or very little) interaction with the walls of the channel appeared; hence the separated cavity formed into an almost spherical conglomerate (cloud) of small bubbles. The cloud is entrained by the flow and violently collapses when it enters a regions of pressure recovery – at t=0 (possibly just a fraction of a second before – about 5 μs are needed for the pressure wave to travel the distance form the collapse point to the surface of the Venturi). At t = 0 ms the damage becomes visible. Stream-wise it lies directly beneath the position of cloud implosion, although some small deviations are possible. From the top view (in the sequence on the left) a single pit was detected, while on the right one, 5 regions of damaged material could be seen (one region (the one at the bottom) contained a cluster of 3 pits). The somewhat random occurrence of the pits implies that they are a result of collapse of single microscopic bubbles, which were present near the Venturi surface – this indirectly confirms the energy cascade explanation of cavitation erosion proposed by Bark et al. [6] and Fortes-Patella [13].

After the collapse (at t > 0) one can see the rebound of the cavity, which did not cause additional damage later on.

3.2 Horseshoe cavitation structure collapse

Cavitating vortices, which appear in a form of a horseshoe shaped structure are known to be responsible for severe erosion in fluid machinery as described by Oba [19]. Franc & Michel [3] conclude that the breaking up of the vortex where the vortex is about to hit the wall and long duration of the impact applied to the wall are the main reasons behind the highly erosive potential of cavitating vortices. Figure 7 shows a sequence of a typical “horseshoe” cloud cavitation structure from the top view.

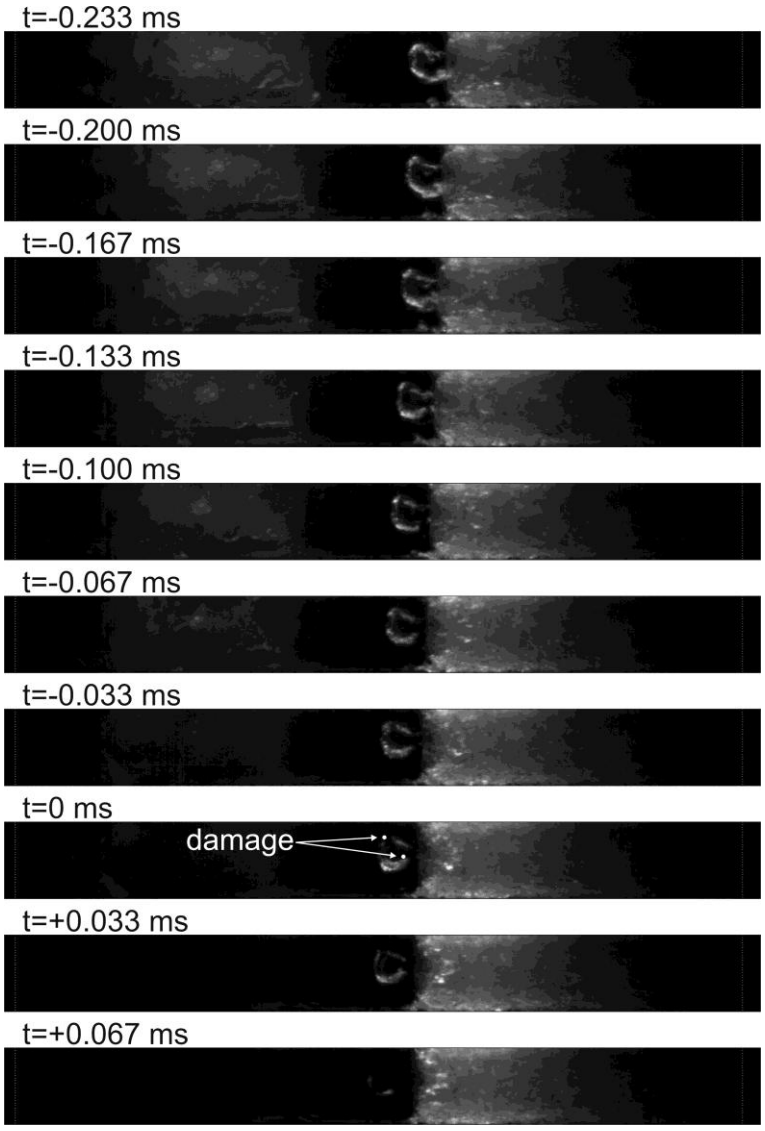

Figure 7: Collapse of a "horseshoe" cavitation structure from top view.

As we see, the cavitating vortex is produced at the closure of the attached cavity – also known as the region where the attached cavity breaks-up. For a vortex to form, it needs to be a closed structure, but it does not need to cavitate over the whole perimeter. When it comes close to the solid structure its loops may attach to the surface, forming a structure that resembles a horseshoe [10].

One can observe that the damage occurs as the vortex begins to break up. Pits appear in the region where the vortex leg touches the surface, thus implying that the breakup of the vortex "leg" and consequent focusing of acoustic energy in space and time (as postulated by van Terwisga et al. [15]) increases the aggressiveness and

causes the formation of the pit.

3.3 "Twister" cavitation structure collapse

Figure 8 shows two sequences of a typical vortex cavitation structure from side (left) and top view (right) – due to its resemblance to a violently rotating column of fluid we denote it as a "twister" cavitation structure.

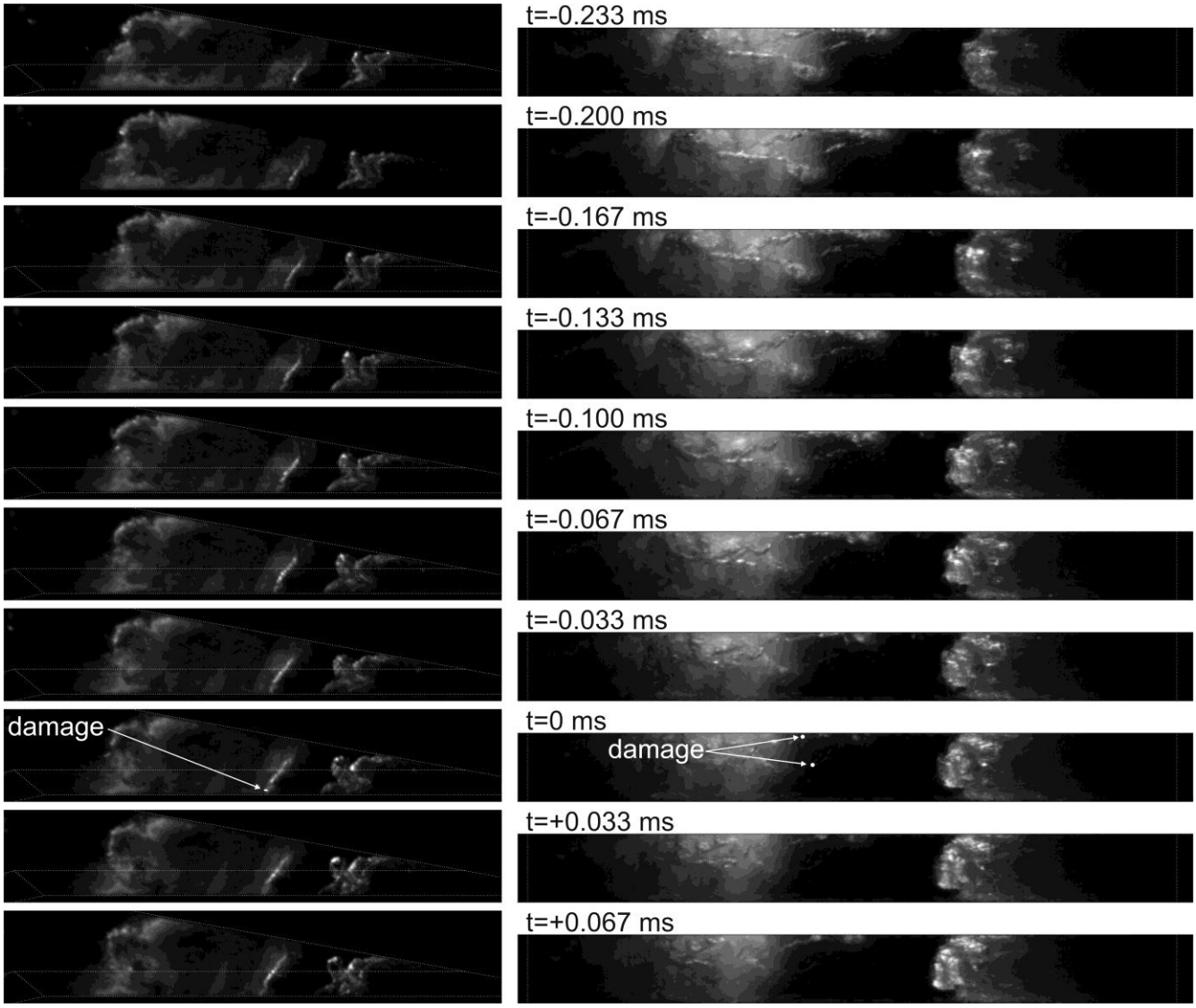

Figure 8: Collapse of a "twister" cavitation structure from side (left) and top view (right).

We believe that the origin of the twister type of cavitation structure is the same as for the horseshoe structure. As

mentioned previously, the vortex is produced at the breakup region, but it does not have to cavitate over the whole circumference – not even over the whole detached circumference. In the present case the vortex first remains liquid. As it is carried downstream by the flow it interacts with the cavitation cloud, what causes it to cavitate. This, like in the case of a breakup of a horseshoe cavitation structure, focuses the acoustic energy towards the solid material.

From Fig. 8 we can again see that the damage is concentrated in the region where the twister touches the solid surface and that it generally occurs when the vortex breaks-up. The rebound of the vortex (at $t > 0$ ms) shows marginal aggressiveness.

3.5 Closure of the attached cavity

In contrary to the phenomena described before we found that the damage also appeared at two instants during the growth of the attached cavity. Figure 9 shows moments during which the damage appears at the attached cavity closure.

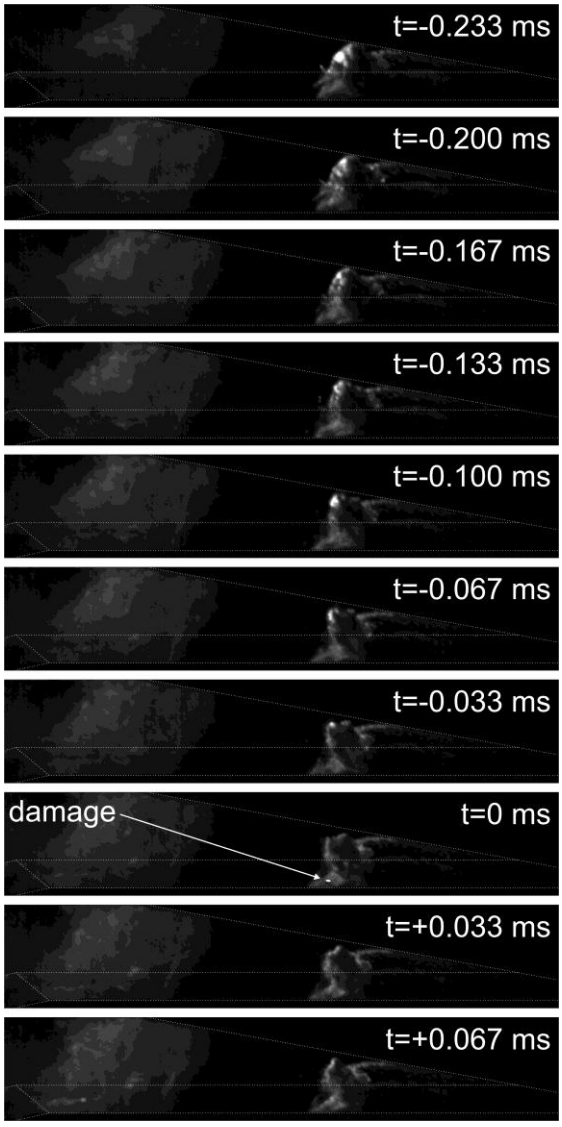

Figure 9: Damage appearance at the closure of the attached cavity from side view.

During the shedding process the outer flow, due to the pressure difference between cavity exterior and interior, deviates towards the solid surface and creates a stagnation point with elevated pressure. The period during which the attached cavity length remains stable is relatively long, the damage, however occurs only randomly during this time. For erosion to occur small scale cavitation structures (single bubbles, which sporadically break off from the attached cavity) must enter the region of higher pressure in the vicinity of the solid surface, and violently collapse. This, however, occurs very rarely due to the fact that the developing re-entrant jet bocks the shedding of small scale structures.

3.5 Cavitation cloud separation

The final erosion mechanism, that we have observed, occurred at the cavitation cloud separation from the attached cavity (Fig. 10).

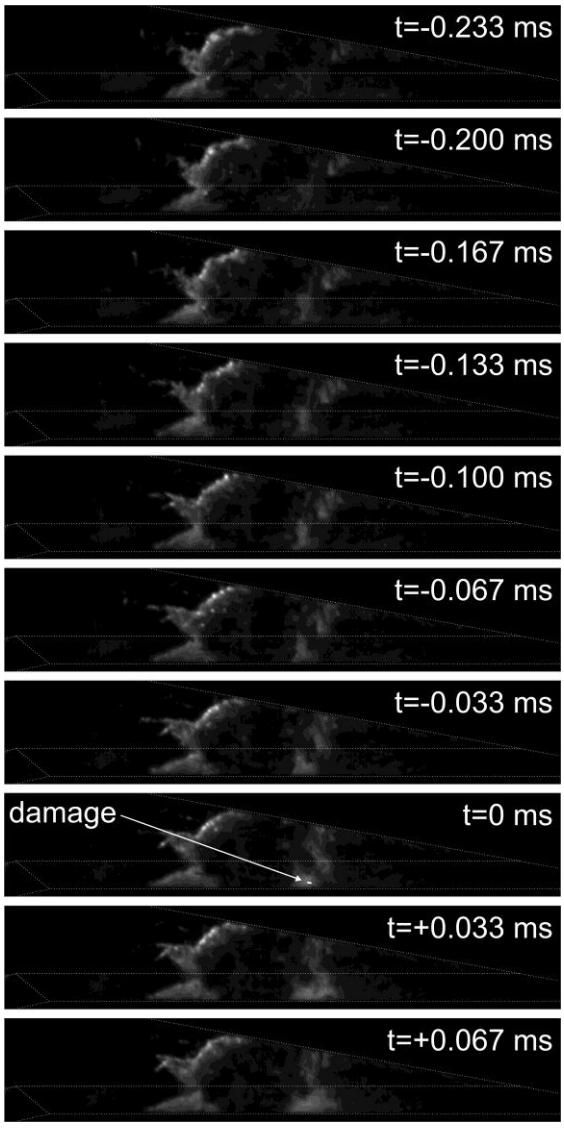

Figure 10: Damage appearance at cavitation cloud separation from side view.

As the re-entrant jet looses momentum it turns upwards cutting the attached cavity into two parts. At this moment the gap between the cloud and the attached cavity is filled up with liquid causing an increase of the

pressure. Again small scale structures that are present in the gap collapse and cause pit formations, what was observed at time t=0 (Fig. 10).

3.6 Some statistics

A relatively large ensemble of the data (over 3000 shedding periods) enables statistical evaluation of the probability of occurrence and the erosive potential of each of the mechanisms. Figure 11 shows the probability that an individual phenomenon will occur during one shedding cycle.

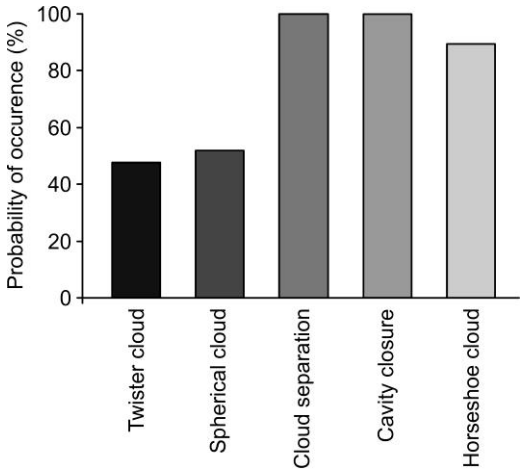

Figure 11: Probability of individual phenomenon to occur during a shedding cycle.

The developed cavitating flow is conditioned by the shedding mechanism, which commences with the formation of the stagnation point at the cavity closure and the separation of the cavitation cloud; hence a 100 % probability of these two events was expected and confirmed by analyzing the images ($P_{c\text{-}c}$ = 100%, $P_{c\text{-}s}$ = 100%). It was found that in the present experiment the horseshoe type cavitation structure forms with a very high probability ($P_{h\text{-}s} \approx 90\%$), what was, considering the small span of the channel, not expected. The separated cloud then takes on two possible forms – it either collapses spherically ($P_{s\text{-}c} \approx 52\%$) and slightly less commonly in a form of a twister ($P_t \approx 48\%$).

Figure 12 (left) shows the probability of the phenomena to cause damage to the foil and the average damage the foil sustained.

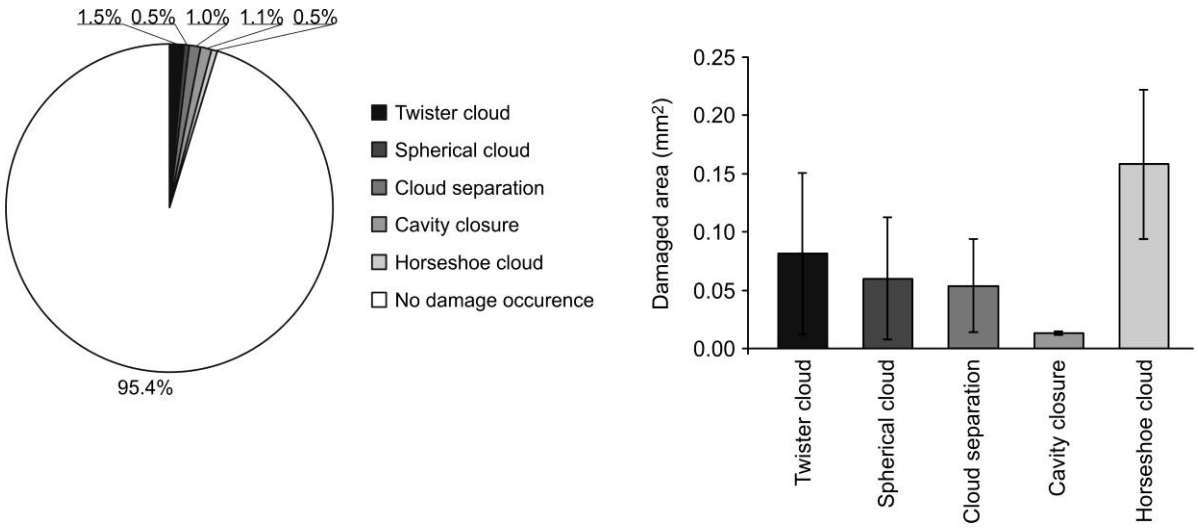

Figure 12: Probability of individual phenomenon to cause damage (left) and the average damage sustained by the foil by individual erosion phenomenon (right).

One can see (Fig. 12, left) that only about every 20th event is actually erosive – even for the present case where the surface was very soft and prone to get damaged. This is in agreement with previous studies, which put the erosive probability to a very low level [20]. The probability for a phenomenon to be erosive is low even when one takes into an account only the cases when the phenomenon actually occurs – then the values $P_{e,t\text{-}c} \approx 12\%$ for the twister cloud, $P_{e,s\text{-}c} \approx 4\%$ for spherical cloud, $P_{e,c\text{-}s} \approx 4\%$ for cloud separation, $P_{e,c\text{-}c} \approx 4\%$ for cavity closure and $P_{e,h\text{-}c} \approx 2\%$ for horseshoe cloud are obtained.

Figure 12 (right) shows the average aggressiveness of individual phenomenon. As one can see the horseshoe cloud collapse is by far the most aggressive one, a related phenomenon – the twister cloud causes on average somewhat less damage. Still aggressive are the spherical cloud collapse and the instant of cloud separation, while the damage caused at the cavity closure was found to me marginal.

The importance of individual phenomenon can be defined by the product of its probability of occurrence and the average damage it causes – Fig. 13 shows the results.

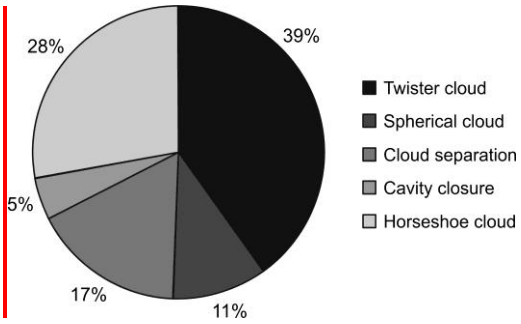

Figure 13: The importance of individual phenomenon.

One can see that, the cloud implosion combined (the sum of the importance of the twister cloud, the horseshoe cloud and the spherical cloud) contributes to almost 80 % of the damage – it is clear why numerous researchers ([13, 15, 21-23] stressed so much importance to it. Between the phenomena the twister cloud implosion is the one to be most considered. It appears frequently and is aggressive; hence it contributes to 39% of the sustained damage. A very important phenomenon is also the horseshoe cloud implosion – mainly due to its aggressiveness. This is also acknowledged in the literature [6]. It is possible that its importance is even greater in channels with wider span [24, 25], where the horseshoe vortex can more easily develop.

Surprisingly important is the cavitation cloud separation from the attached part of the cavity, which was, prior to this study, probably mistaken for the mechanism of cavity closure, since they both contribute to damage in a similar region. The later is of an insignificant importance.

4 Discussion

In the discussion we will follow the mechanisms as they would appear during one period of shedding. Figure 14 represents the time evolution and the variants of the shedding that lead to different mechanisms of cavitation induced damage. The instants (C, E, H, L and O) when the damage occurs are highlighted by the darker colour.

As mentioned in the introduction, the general consent is that the collapse of the macroscopic cavitation structure cannot damage the material directly, due to the fact that the energy is not concentrated enough. The potential energy contained in a macro cavity is transformed into the radiation of acoustic pressure waves, and further on into the erosive power contained of the micro-scale cavitation structures or single bubbles. Two theories describe the last stages of life of a microscale cavitation structure:

- if we assume that the bubble will collapse in the form of a micro-jet we can estimate its velocity according to the theory by Plesset & Chapmann [26] and to experimetal and numerical work by Chanine [27]:

$$v_{m-j} = k \cdot \frac{h}{R_0} \sqrt{\frac{p_\infty - p_v}{\rho}} . \qquad (2)$$

R_0 is the initial bubble diameter and h is the initial distance of the bubble center from the wall. Chahine [27] puts the $k \cdot \frac{h}{R_0} = 4.6$ for a bubble 0.5 mm in radius at a standoff distance of 0.375 mm. It is common to obtain velocities of the micro-jet in the order of several hundred m/s. The pressure induced on the solid material is the water hammer pressure reduced by the efficiency of the inpact, which lies at 60% according to Chahine [27]:

$$p_{w-h} = 0.6 \cdot c \cdot \rho \cdot v_{m-j} , \qquad (3)$$

where c is the liquid sonic velocity – one can easily calculate the great erosive potential of such collapse.

- The second widely accepted mechanism that takes place in creating a pit is the spherical collapse of an even smaller bubble. The pressure field, in terms of the distance from the bubble center and the time $p_{m-b}(r,t)$, can be determined by solving the Reyleigh-Plesset equation [3]. It results in:

$$p_{m-b}(r,t) = p_\infty + (p_\infty - p_v)\left(\frac{R}{3r}\left[\frac{R_0^3}{R^3} - 4\right] - \frac{R^4}{3r^4}\left[\frac{R_0^3}{R^3} - 1\right]\right). \quad (4)$$

The results put the maximal pressure in an order of several hundred MPa – again one can appreciate the high pressure and erosive potential of such collapse.

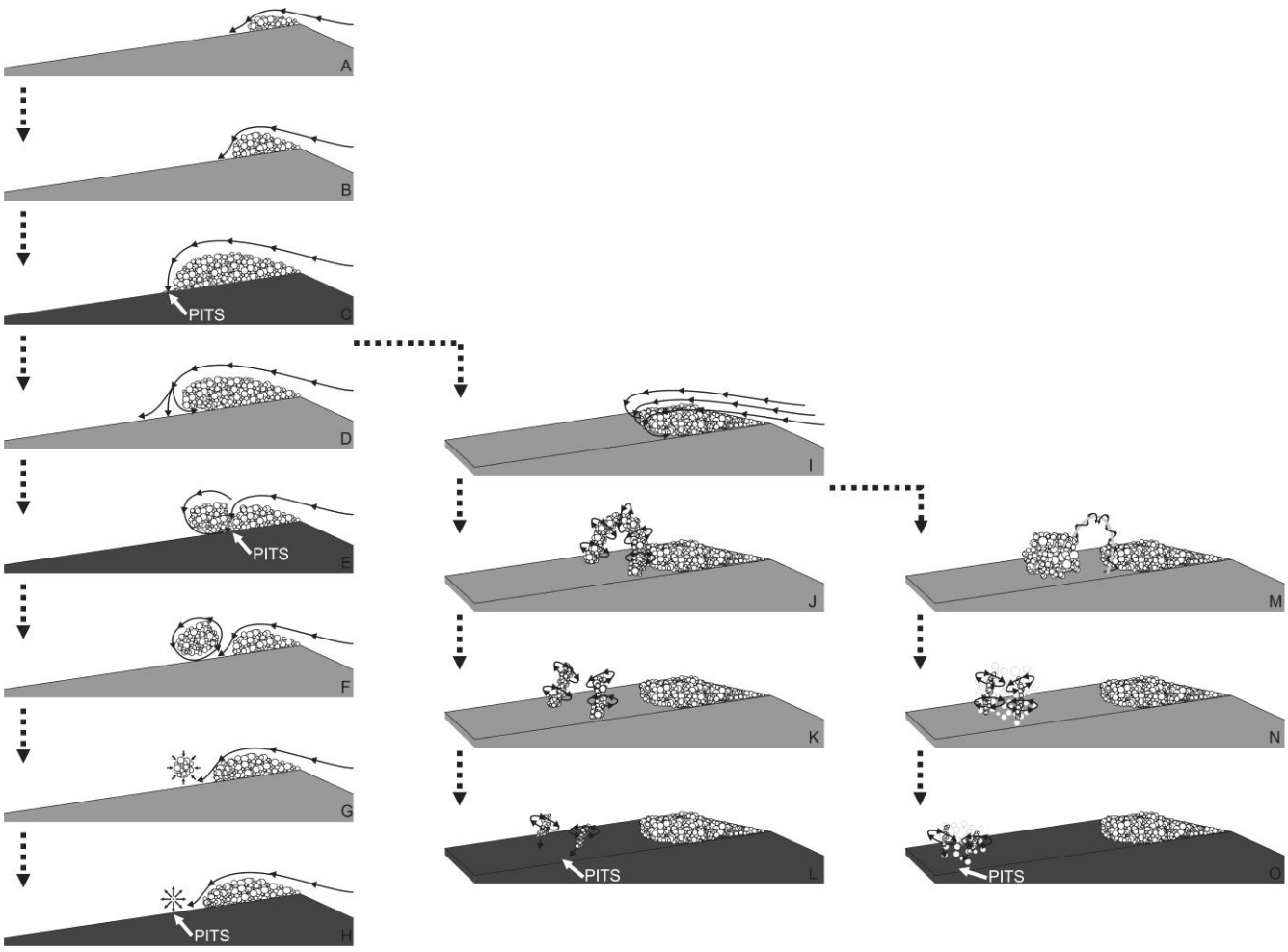

Figure 14: Schematic representation of observed mechanisms that lead to occurrence of cavitation erosion (the inner structure and the size of the bubbles may not correspond to reality). The instants of damage appearance are denoted by the darker colour. An arrow marks the region where the pits occur.

As already mentioned the in the introduction, the shedding process begins with the growth of the attached cavity (Fig. 14, A and B). As the pressure difference between the outer (liquid) flow and the cavity interior rises it forces the liquid flow to deviate towards the cavity and the solid surface beneath it. As the flowline hits the surface a stagnation point forms (Fig. 14, C) and the pressure at the cavity closure increases from slightly above vapour pressure to roughly the sum of stagnation pressure and the vapour pressure:

$$p_{closure} \approx p_v + \frac{\rho v_j^2}{2}, \qquad (5)$$

where v_j is the liquid flow velocity at the cavity closure (approximately 17m/s in the present experiment). The pressure at the closure would then be $p_\infty \approx 150000$ Pa. This implies that the small cavitation structures or bubbles which enter this region of elevated pressure will violently collapse. The intensity of the microstructure collapse can be estimated by Eqns. 2 to 4. If we assume that a bubble, 1 mm in diameter with its center 0.375mm from the wall (known to be the most aggressive case [27] we get micro jet velocity in the order of 56 m/s. The pressure induced on the solid material is then approximately $p_{w\text{-}h} \approx 51$ MPa - one can easily appreciate the great erosive potential of such collapse. For the other approach we can assume that the initial diameter of the bubble is 0.1 mm, its minimal size of is $1/20^{th}$ of its initial size [3] and its center lies 0.0375 mm from the wall (the same non-dimensional bubble standoff distance as for the case of micro-jet approach). Again we take $p_\infty = 150000$ Pa as the pressure at the closure. The results puts the pressure to $p_{m\text{-}b} \approx 26$ MPa and again points to an aggressive collapse. Although the values point to a very aggressive mechanism of cavitation erosion the probability of its occurrence is low, due to the fact that the re-entrant jet prevents the bubbles to enter the region of elevated pressure.

After the stagnation point is established the jet splits into the part that follows the main flow direction and the part that penetrates the cavity and travels upstream – the re-entrant jet (Fig. 14, D). As the jet turns upwards and cuts the attached cavity it creates a liquid gap between the, now separated, attached cavity and the cavitation

cloud (Fig. 14, E).

In our recent numerical work by Wang et al. [28] we have shown that as the cavitation cloud separates (as the gap between the structures forms) the pressure peak occurs just after the cavitation breaks off (in a very confined region). It is still not clear what causes the relatively significant increase of pressure. As the gap forms, it is quickly filled up by the surrounding liquid, however it is unlikely that the mechanism is the formation of the stagnation point by the emerging re-entrant jet – if this was so, the attached cavity would not begin to grow. Possibly the mechanism is simply that the pressure increases to the level of the pressure surrounding the cavitation structure, which is somewhat higher than the pressure inside it. In the simulation [28] the pressure locally increases to 410000 Pa. This is of course, too low to cause damage directly, but if one again uses the reasoning given before (Eqns. 2-4) and assumes that bubbles 1 mm in diameter are shed from the attached cavity and that they collapse at a standoff distance of 0.375 mm, one gets: $v_{m\text{-}j} \approx 93$ m/s, $p_{w\text{-}h} \approx 84$ MPa and $p_{m\text{-}b} \approx 73$ MPa. The numbers again point to a very aggressive bubble collapse, which can cause damage to the solid material.

The next step in the shedding process is the formation of a cavitation cloud, which can take on very different shapes and sizes. In an ideal situation it remains almost spherical (Fig. 14, F). As it is carried by the flow to a higher pressure region (Fig. 14, G) it can violently collapse causing an emission of a shock wave (Fig. 14, H). At a collective bubble collapse cascades of implosions are usually present – the pressure wave emitted at one bubble collapse tends to enhance the collapse of bubbles in its vicinity. The shock wave usually tends to travel inwards and due to quasi-spherical symmetry focuses to the cloud center, thus increasing the aggressiveness of the collapse.

The shock waves emitted at the cloud collapse are in the order of several MPa. Measurements on a simple hydrofoil geometry were performed by Bohm [29] who obtained a maximum of 1.4 MPa. These were successfully reproduced numerically by Dular & Coutier-Delgosha [23]. Theoretical work by Shimada et al. [30] put it in the range between 4 and 12 MPa. In our simulations of the flow in the present configuration [28] we could observe several fluctuations before the pressure reached the highest point, which implies that the cavity

collapse is not instantaneous – the maximum was predicted to reach 1.13 MPa.

If we again consider the possibility that small singe bubbles are present near the wall at the moment of cavitation cloud collapse (Eqns. 3 to 5), with 1.13 MPa as the p_{∞}, we come to loads of $p_{w\text{-}h} \approx 139$ MPa for the theory of the micro-jet impact and to $p_{m\text{-}b} \approx 201$ MPa for the idea of the spherical micro-bubble collapse. Both values show the great potential of spherical cloud collapse to be one of the primary mechanisms behind cavitation erosion process.

As already mentioned the separated cloud is rarely spherical due to vortices that are produced in the break up region (Fig. 14, J). It is common that the cavity closure line bends due to the side wall effects, such as the presence of the boundary layer. As a consequence the re-entrant jet is deflected towards the mid-span region of the channel – a process similar to the cavitation shedding on hydrofoils with spanwise variation [31-33]. This causes a cavity breakup in the middle of the span of the channel. It then rolls up, due to the circulation induced by the re-entrant jet, and forms a distinctive U shape – termed horseshoe cavitation cloud by Joussellin et al. [34].

The large scale primary spanwise vortices were studied in detail by Pereira et al. [9] who observed them with four cameras from different viewing angles, thus allowing for a 3D reconstruction of the structures and by Kawanami et al. [10], who used holography to show that the cavity consists of vortex core and numerous bubbles surrounding it. They showed that while the horseshoe structure is carried downstream it usually splits at the top – likely due to instabilities occurring on the cavity liquid interface. The remaining "legs" collapse further downstream (Fig. 14, K and L). Presumably due to self induction, the vorticity is attracted towards the solid surface, thereby focusing the bubbly clouds to collapse along the axis of the legs in the direction toward the surface. The final collapse is triggered by the emission of a shock wave of the first collapsing bubble, thus inducing a synchronized collapse of the bubble cloud.

The focusing of the energy was first proposed by Bark et al. [6]. A similar explanation was recently suggested by van Rijsbergen et al. [1]. Based on acoustic emission measurements they came to a conclusion – that only cloud implosions where the emitted shock wave has a clear orientation (the highest impact occurs when the wave front

is directed toward the wall) lead to stress on the surface and erosion. This was also indirectly shown in high fidelity simulations by Schmidt et al. [35] (simulations of the flow on the present geometry by Wang et al. [28] were not able to resolve the horseshoe cavitation vortex).

Experimental data for cavitation on a twisted hydrofoil at flow velocity of 12 m/s by Foeth et al. [7], and simulations by Schmidt et al. [35] and Bin et al. [36] show that the vortices evolve to a cavitating structure approximately 40 mm in diameter with leg diameter of maximum 12 mm. In the preset experiment, we are dealing with much smaller horseshoe clouds – maximum lies at about 9 mm in diameter and leg diameter of 4 mm but at a higher flow velocity (25 m/s). According to Bark et. al [6] the structure caries a potential energy of:

$$E_p = V_{cav} \cdot \left(p_\infty - p_v \right). \tag{6}$$

The pressure difference (p_∞ - p_v) is a function of the square of flow velocity, one can therefore estimate the relationship between the energies as:

$$\frac{E_{p,big}}{E_{p,small}} = \frac{V_{cav,big} \cdot v_{big}^2}{V_{cav,small} \cdot v_{small}^2} = 6.4, \tag{7}$$

where v_{big} and v_{small} are the flow velocities for the larger [7] and the present case (12 and 25 m/s, respectively). For the case of twisted hydrofoil a maximum pressure of 13 MPa was predicted Schmidt et al. [35] . Considering Eqn. 7 one can therefore expect the pressure in the present configuration to lie in the order of 2 MPa. Taking this value into an account and considering Eqns. 2 to 4 we get stresses on the solid boundaries which surpass all the previously mentioned mechanisms, $p_{w\text{-}h} \approx 189$ MPa for the theory of the micro-jet impact and to $p_{m\text{-}b} \approx 371$ MPa for the collapse of the spherical microbuble.

The final phenomenon that we observed during the shedding process is characterized by the fact that the

spanwise vortex remains liquid as it separates from the attached cavity (Fig. 14, M). The mechanism of its origin is believed to be the same as for the horseshoe cloud, but the pressure inside its core remains at a somewhat higher level, which prevents it to cavitate. The formation of such vortex usually follows the separation of a quasi-spherical cavitation cloud – both within one single shedding period. The existence of a significant slip velocity between the vapour and the liquid phase (as it was recently shown by Coutier-Delgosha et al. [37] causes the vortex to catch up with the cloud and to interact with it (Fig. 14, N). The bubbles are attracted by the low pressure vortex core and are transported towards the surface of the Venturi, where they again collectively collapse (Fig. 14, O). Compared to the classical horseshoe cavitation cloud the "twister" cloud is somewhat smaller and usually only a single "leg" forms. As a consequence one can expect a somewhat lower potential energy of such structure. An average twister measured 3 mm in diameter and was 9 mm long. Following the previous reasoning we get $\frac{E_{p,big}}{E_{p,small}} = 11.3$ and the pressure on the surface of 1.1 MPa. This leads to $p_{w\text{-}h} \approx 142$ MPa for the theory of the micro-jet impact and to $p_{m\text{-}b} \approx 208$ GPa at the collapse of the spherical microbuble.

The discussion is summarized in Tab. 1 where the measured average damage A_{dam} and the estimated average load ($p_{w\text{-}h}$ and $p_{m\text{-}b}$) on the surface are shown for individual discussed mechanism of cavitation erosion.

Table 1: Measured average damage and estimated loads on the surface.

	$\mathbf{A_{dam}}$	$\mathbf{p_{w\text{-}h}}$	$\mathbf{p_{m\text{-}b}}$
	mm^2	**MPa**	**MPa**
Horseshoe cloud	0.158	189	371
Twister cloud	0.081	142	208
Spherical cloud	0.060	139	201
Cloud separation	0.054	84	73
Cavity closure	0.013	51	26

Of course one cannot take the values in Tab. 1 as absolute, but looking at it from a relative perspective we can see that the reasoning in the discussion correctly predicts the aggressiveness of the erosion mechanisms. If one looks at the numbers from an absolute point of view also a conclusion that indeed only mechanisms associated with collapsing cavitation cloud (horseshoe cloud, twister cloud and spherical cloud) are important in technical applications where materials with higher yield strength are used. Yet the stresses induced at the instant of cavitation cloud separation and at the cavity closure region could also be much higher in other geometries and should therefore not be considered irrelevant.

Interestingly, one can also conclude that cavitating vortex is present at some point during each of the observed phenomena. It is inertia driven to meet the conflicting boundary condition at the surface of the sheet cavity and its closure point. At the instant of shedding, circulation arises around a vapor cloud and separates it from the attached cavity. It manifests in form of a horseshow when it cannot end in the fluid or forms a twister when the horseshoe structure is not cavitating or only partially cavitating. Acknowledging the relationship between the presence of the vortex structures and cavitation erosion therefore seems to be of a critical importance.

5 Conclusions

The study presents an original experimental technique where the cavitation structures and cavitation damage are observed simultaneously at a relatively high frame rate (30000 fps in the present case).

Based on original experiments and past experimental, theoretical and numerical studies several mechanisms of cavitation erosion were discussed. It was shown that the process is much more complex than previously thought. Some cavitation phenomena were, for the first time, related to cavitation erosion – for example the development and focused collapse of the twister cloud and damage occurrence in the region of cavitation cloud separation.

It was found in experiment that indeed the cavitation cloud shedding process is the needed condition for the damage occurrence – almost 80% of the damage can be contributed to mechanisms of cloud collapse (spherical, horseshoe and twister). Among them the twister type is the one to be the most considered - due to its aggressiveness and the probability of damage appearance. Horseshoe type cavitation structure develops in almost

every period and was found to be very aggressive, but its probability to create a pit is low. Interestingly, a very limited amount of damage can be contributed to collapses of micro scale structures in the closure region of the attached cavity. Its importance was probably overestimated due to the mix-up with the damage that occurs at cavitation cloud separation – both mechanisms damage the surface in a similar area.

Acknowledgments

The study was performed under a grant by the Slovenian Research Agency (ARRS) – High Fidelity Simulations and Experiments for the Prediction of Cavitation Erosion (J2—6774). The test facility was developed with a continuous financial support by the European Space Agency (ESA).

References

[1] M. van Rijsbergen, E.J. Foeth, P. Fitzsimmons, A. Boorsma, High speed video observations and acoustic impact measurements on a NACA0015 foil, In Proceedings of the 8th International Symposium on Cavitation, August 13-16, Singapore (2012).

[2] M. Petkovšek, M. Dular, Simultaneous observation of cavitation structures and cavitation erosion, Wear 300 (1/2) (2013) 55-64

[3] J.P. Franc, J.M. Michel, Fundamentals of Cavitation, Kluwer Academic Publishers (2004).

[4] M. Dular, I. Khlifa, S. Fuzier, M. Adama Maiga, O. Coutier-Delgosha, Scale effect on unsteady cloud cavitation, Exp. Fluids 53, (2012) 1233–1250.

[5] G.E. Reisman, Y.C. Wang, C.E. Brennen, Observations of shock waves in cloud cavitation, Journal of Fluid Mechanics 355 (1998) 255-283.

[6] G. Bark, J. Friesch, G. Kuiper, J.T. Ligtelijn, Cavitation Erosion on Ship Propellers and Rudders. In Proceedings of the 9th Symposium on Practical Design of Ships and Other Floating Structures, Luebeck-Travemuende, Germany (2004).

[7] E.J. Foeth, T. van Terwisga, C.van Doorne, On the Collapse Structure of an Attached Cavity on a Three-Dimensional Hydrofoil, ASME J. Fluids Eng. 130(7), (2008) 071303.

[8] A. Boorsma, S. Whitworth, Understanding details of cavitation, In Proceedings of the 2nd International Symposium on Marine Propulsors, Hamburg, Germany (2011) .

[9] F. Pereira, F. Avellan, J.M. Dupont, Prediction of Cavitation Erosion: an Energy Approach, ASME J. Fluids Eng 120 (4) (1998) 719-727.

[10] Y. Kawanami, H. Kato, H. Yamaguchi, M. Maeda, S. Nakasumi, Inner structure of cloud cavity on a foil section, JSME International Journal 45 (3) (2002) 655-661.

[11] F.G. Hammitt, Observations on Cavitation Damage in a Flowing System, Trans. ASME, J. of Basic Engineering, 3 (1963).

[12] Y.C. Wang, C.E. Brennen, Shock wave development in the collapse of a cloud of bubbles. ASME FED Cavitation and Multiphase flow, 194 (1994).

[13] R. Fortes-Patella, J.L. Reboud, L. Briancon-Marjollet, A phenomenological and numerical model for scaling the flow aggressiveness in cavitation erosion. EROCAV Workshop, Val de Reuil, France (2004).

[14] G. Bark, N. Berchiche, M. Grekula, Application of principles for observation and analysis of eroding

cavitation. The EROCAV observation handbook, Edition 3.1, (2004)

[15] T. van Terwisga, P.A. Fitzsimmons, L. Ziru, E.J. Foeth, Cavitation Erosion – A review of physical mechanisms and erosion risk models. In Proceedings of the 7th International Symposium on Cavitation, August 17-22, Ann Arbor, Michigan, USA (2009).

[16] F. Brand, Ein physikalisches Verfahren zur Bestimmung von geloesten und ungeloesten Gasen in Wasser, Voith Forschung und Konstruktion 27 (1981).

[17] F.B. Peterson, Hydrodynamic cavitation and some considerations of the influence of free gas content, in: Proceedings of the 9th Symposium on Naval Hydrodynamics, (1972).

[18] R.E.A. Arndt, A.P. Keller, Free gas content effects on cavitation inception and noise in a free shear flow, in: Proceedings of the IAHR Symposium Two Phase Flow and Cavitation in Power Generation Systems, Grenoble, (1976).

[19] R. Oba, The severe cavitation erosion. In Proc. Of the 2nd International Symposium on Cavitation, April 5-7, Tokyo, Japan (1994).

[20] R.T. Knapp, Recent investigations of the mechanics of cavitation and cavitation damage, Trans. ASME 75 (8) (1955) 1045–1054.

[21] M. Dular, B. Bachert, B. Stoffel, B. Sirok, Relationship between cavitation structures and cavitation damage. Wear 257 (2004) 1176–1184.

[22] M. Dular, B. Stoffel, B. Sirok, Development of a cavitation erosion model. Wear 261(5–6) (2006) 642–655.

[23] M. Dular, O. Coutier-Delgosha, Numerical modelling of cavitation erosion. Int. J. Numer. Meth. Fluids 61 (2009) 1388–1410.

[24] M.S. Plesset, R.B. Chapman, Collapse of an innitially spherical vapour cavity in the neighbourhood of a solid boundary. J. Fluid Mech. 47 (1971) 283–290.

[25] T. Keil Theoretische und experimentelle Untersuchungen der Schicht- und Wolkenkavitation. PhD. Thesis, Technische Universität Darmstadt (2014).

[26] P.F. Pelz, T. Keil, G. Ludwig, On the Kinematics of Sheet and Cloud Cavitation and Related Erosion. In Advanced Experimental and Numerical Techniques for Cavitation Erosion Prediction. Fluid Mechanics and Its Applications 106. Edts.: Kim, K.H., Chahine, G., Franc, J.P., Karimi, A., Springer 2014.

[27] G.L. Chahine, Modeling of Cavitation Dynamics and Interaction with Material. In Advanced Experimental and Numerical Techniques for Cavitation Erosion Prediction. Fluid Mechanics and Its Applications 106. Edts.: Kim, K.H., Chahine, G., Franc, J.P., Karimi, A., Springer 2014.

[28] J. Wang, M. Petkovšek, H. Liu, B. Sirok, M. Dular, Combined numerical and experimental investigation of the cavitation erosion process. ASME J. Fluids Eng 137 (5) (2015) 1-9.

[29] R. Böhm, Erfassung und hydrodynamische Beeinflussung fortgeschrittener Kavitationsustände und ihrer Aggressivität. PhD Thesis, Technische Universität Darmstadt, Darmstadt (1998).

[30] M. Shimada, T. Kobayashi, Y. Matsumuto, Dynamics of cloud cavitation and cavitation erosion. In

Proceedings of the ASME/JSME Fluids Engineering Division Summer Meeting, San Francisco, USA, 1999.

[31] D.F. de Lange, G.J. de Bruin, Sheet cavitation and cloud cavitation, re-entrant jet and three-dimensionality. Applied Scientific Research 58 (1998) 91–114.

[32] K.R. Laberteaux, S.L. Ceccio, Partial cavity flows. Part 2. Cavities forming on test objects with spanwise variation, Journal of Fluid Mechanics 431 (2001) 43–63.

[33] M. Dular, R. Bachert, C. Schaad, B. Stoffel, Investigation of re-entrant jet reflection at an inclined cavity closure line. European journal of mechanics: B-Fluids 26 (5) (2007) 688-705.

[34] F. Joussellin, Y. Delannoy, E. Sauvage-Boutar, B. Goirand, Experimental investigations on unsteady attached cavities. AMSE-FED 116 (1991) 61–66.

[35] S.J. Schmidt, I.H. Sezal, G.H. Schnerr, M. Thalhamer, Shock waves as driving mechanism for cavitation erosion. In Proceedings of the 8th International Symposium on Experimental and Computational Aerothermodynamics of Internal Flows, Lyon, France, 2007.

[36] J. Bin, L. Xianwu, W. Yulin, P. Xiaoxing, D. Yunling, Numerical analysis of unsteady cavitating turbulent flow and shedding horse-shoe vortex structure around a twisted hydrofoil. International Journal of Multiphase Flow 51 (2013) 33–43.

[37] O. Coutier-Delgosha, I. Khlifa, M. Hocevar, S. Fuzier, A. Vabre, K. Fezzaa, Velocimetry in both phases of a cavitating flow by fast X-ray imaging. Bulletin of the American Physical Society 57 (2012).

Highlights

Cavitation structures and cavitation erosion were simultaneously observed.
5 distinctive erosion mechanisms were determined.
The focused collapse of the twister cloud and the damage occurrence was observed.
80% of the damage can be contributed to mechanisms related to cavitation cloud collapse.